New Journal of Physics
The open access journal for physics

Impact of track structure calculations on biological treatment planning in ion radiotherapy

Thilo Elsässer[1], **Richard Cunrath, Michael Krämer and Michael Scholz**

Gesellschaft für Schwerionenforschung (GSI), Planckstrasse 1, 64291 Darmstadt, Germany
E-mail: t.elsaesser@gsi.de

New Journal of Physics **10** (2008) 075005 (17pp)
Received 20 February 2008
Published 28 July 2008
Online at http://www.njp.org/
doi:10.1088/1367-2630/10/7/075005

Abstract. Treatment planning for ion therapy requires precise knowledge about the biological effectiveness of particle beams, which is strongly determined by the microscopic radial energy deposition around individual ion tracks. We analyse different amorphous track structure models based on simple analytical formulae as well as on radial dose distributions derived by means of Monte Carlo simulations. Moreover, these track structure representations are used as input for the local effect model (LEM) in order to determine their impact on the relative biological effectiveness (RBE) of cell inactivation. It demonstrates the relevance of the inner part of the ion track with a radius of the order of a few nanometres. We show that simple analytical formulae for the radial dose distributions give good results for the prediction of cell inactivation. However, they strongly depend on the assumptions about the local dose in the track core. Additionally, we discuss the interdependence of track structure calculations with other model constituents such as target size and the choice of the biological input data for conventional photon irradiation.

[1] Author to whom any correspondence should be addressed.

Contents

1. Introduction

In recent years, heavy particles such as swift carbon ions have gained in importance for tumour therapy due to two desirable properties. The beneficial energy deposition with the largest dose in the tumour region and the advantageous biological effectiveness of heavy ions offer enormous potential for treatment with an as yet unmatched high tumour conformity for many indications [1]. First clinical results show a promising tumour control probability combined with a low risk of normal tissue complications [2, 3]. Based on this prospect, several dedicated clinical facilities are being constructed, approved or planned all over the world [4].

Besides the favourable absorbed dose distribution offered by charged particles due to the high-energy density at the end of their penetration depth in the so-called Bragg peak region, the large biological efficacy of heavy ions constitutes the major advantage of carbon ion therapy. It is usually expressed in terms of the relative biological effectiveness (RBE), which quantifies the different biological response of ions relative to conventional x-ray irradiation. It is defined by the ratio of the x-ray dose versus the dose delivered by ions required to achieve the same biological effect.

It is of particular importance to realize that the RBE depends on numerous physical and biological parameters such as ion species, ion energy and dose as well as the biological endpoint and the tissue type under consideration [5, 6]. Therefore, a comprehensive experimental database covering all conceivable parameter configurations is all but impossible. In the first therapy projects with heavy ions in Berkeley, USA [7] and Chiba, Japan [8], this challenge was approached by measuring cell inactivation *in vitro* and relating that experience to the clinical case in order to determine the clinical RBE. In both projects, it is assumed that the clinical RBE does not change with dose, ion species or tissue type. The first treatment planning system considering these dependencies was established in the GSI pilot project by means of the local effect model (LEM) [9, 10]. Its three main constituents comprise the cell nucleus as the sensitive target, the conventional photon response curve for the biological characteristics and the radial dose deposition around the ion track as an effective consideration of physical and chemical effects. All these ingredients are known to be essential for an assessment of radiobiological effects induced by ion irradiation. However, the accuracy of their quantification is limited due to a lack of experimental data, e.g. survival at high doses or dose deposition at small distances

from the track centre. Therefore, reasonable and simple models including several assumptions had to be developed to describe the relevant input data.

In this paper, we focus on the radial dose deposition usually referred to as track structure, which accounts for the ionization density around the centre of ion tracks and subsequent chemical processes. In recent decades, numerous models have been developed to calculate the energy deposition of particles either *ab initio* by Monte Carlo simulations of primary interaction events followed by a detailed tracking of secondary electrons [11]–[13] or by analytical amorphous track structure models [14]. Although the latter are supposed to be inferior to Monte Carlo models in terms of precision, their high computational speed and simplicity makes them good candidates for purposes in ion therapy, where a large number of treatment plans must be calculated. Moreover, for mechanistic modelling, accurate quantification of physical processes such as the angular distribution of secondary particles is difficult and density-related effects like polarization screening or plasmon excitation are considerably unexplored experimentally.

In the following, we compare different analytical track structure models to radial dose distributions that have been derived by integrating the energy deposition events generated by Monte Carlo simulations. Both approaches result in an amorphous description of the energy deposition around ion tracks either without explicitly considering the microscopic substructure due to secondary electrons or by averaging them out along the tracks. Subsequently, the different descriptions of the radial dose distribution are used as input for the LEM in order to calculate cell inactivation probabilities. We have chosen the human salivary gland (HSG) cell line as biological model system, since it is the basis of treatment planning at the carbon ion treatment centres at Hyogo and Chiba [15].

In the last part, we discuss the interplay between different model parameters like the photon dose response curve and the geometric structure of the sensitive target. Depending on the choice of these parameters, the significance of deviations between track structure models varies rather strongly. For this discussion, the ideas of the microdosimetric kinetic model (MKM) [16, 17] and the approach by Katz [18] for the calculation of the biologically effective dose are taken into account.

2. LEM

The LEM assumes that the biological effect of irradiation is entirely determined by the spatial local dose distribution inside the cell nucleus. Since the biological damage mainly results from ejected electrons (δ-electrons), which are generated by photons as well as ions, we can infer the resulting damage of heavy ions from the corresponding experiments with x-rays. The accumulated local dose from different tracks can be calculated for small subvolumes individually by using a track structure model. With the knowledge about the deposited dose, the resulting biological damage can be extrapolated from data of x-ray experiments for each subvolume and integrated over the entire cell nucleus.

We assume that the number of lethal events N after x-irradiation follows Poisson statistics, since the lethal events are expected to be distributed randomly in the sensitive target. Therefore, the fraction of surviving cells after x-irradiation can be written as

$$S_x(D) = \mathrm{e}^{-N_x(D)}, \tag{1}$$

where $S_x(D)$ is the result of a measurement and the average number of lethal events $N_x(D)$ is readily derived by

$$N_x(D) = -\ln S_x(D). \tag{2}$$

Additionally we introduce the dose-dependent event density for x-irradiation, $\nu_x(D)$:

$$\nu_x(D) = \frac{N_x(D)}{V}, \tag{3}$$

with V being the target volume.

For particle irradiation, the dose distribution is highly inhomogeneous and we must consider the three-dimensional (3D) local dose $d(x, y, z)$ to calculate the average number of lethal events:

$$N_{\text{ion}} = \int_{V_{\text{nucleus}}} \mathrm{d}V \nu_{\text{ion}} \left[d\,(x, y, z)\right], \tag{4}$$

where ν_{ion} denotes the lethal event density after ion radiation. According to the main idea of the LEM, the local dose effect is independent of the radiation quality and we can set $\nu_{\text{ion}}(d) = \nu_x(d)$. Using equations (2) and (3), we find:

$$N_{\text{ion}} = -\int_V \mathrm{d}V \frac{\ln S_x\left[d\,(x, y, z)\right]}{V}. \tag{5}$$

Equation (5) represents the most general formulation of the LEM and illustrates the relation of the biological effect of particle irradiation to the effect of photon irradiation. We can identify the three input quantities, namely the volume V of the sensitive target, the local dose distribution d and the experimental survival curve S_x after x-irradiation. Figure 1 shows a sketch of the calculation of equation (5). The positions of ion tracks are randomly distributed over the cell nucleus according to Poisson statistics with the average number of traversals as the mean value of the Poissonian.

Since the focus of this work is devoted to the radial dose distribution, we only briefly summarize the other two model constituents. It is well accepted that the DNA in the cell nucleus is the critical target for cell inactivation. If we assume that the sensitive sites are distributed homogeneously over the cell nucleus and that they exhibit the same radiosensitivity, we can take the effective geometrical area A of the cell nucleus and its height h to calculate the sensitive volume V. In general, we need to consider the effective size $A = \pi r_{\text{n}}^2$, which is smaller than the arithmetic mean of the size distribution of cell nuclei [19] accounting for inhomogeneities in DNA density.

Generally, any representation of the cell survival curve after photon irradiation can be used as the input of the LEM. In the following, we focus on the linear-quadratic approach to parameterize the cell inactivation curve, since it is well accepted and most widely used in literature. However, experiments show that a purely linear-quadratic model overestimates the radiation effect for high doses of the order of 10 Gy [20], and a modification must be introduced to account for this behaviour. We assume as a simple approximation that above a threshold dose D_{t} the survival curve turns from the shouldered form into a purely exponential part. For even higher doses above a few hundred Gy, we need to consider cluster effects due to the enormous ionization densities in the track centre resulting in nearby single strand breaks (SSBs) [21]. If

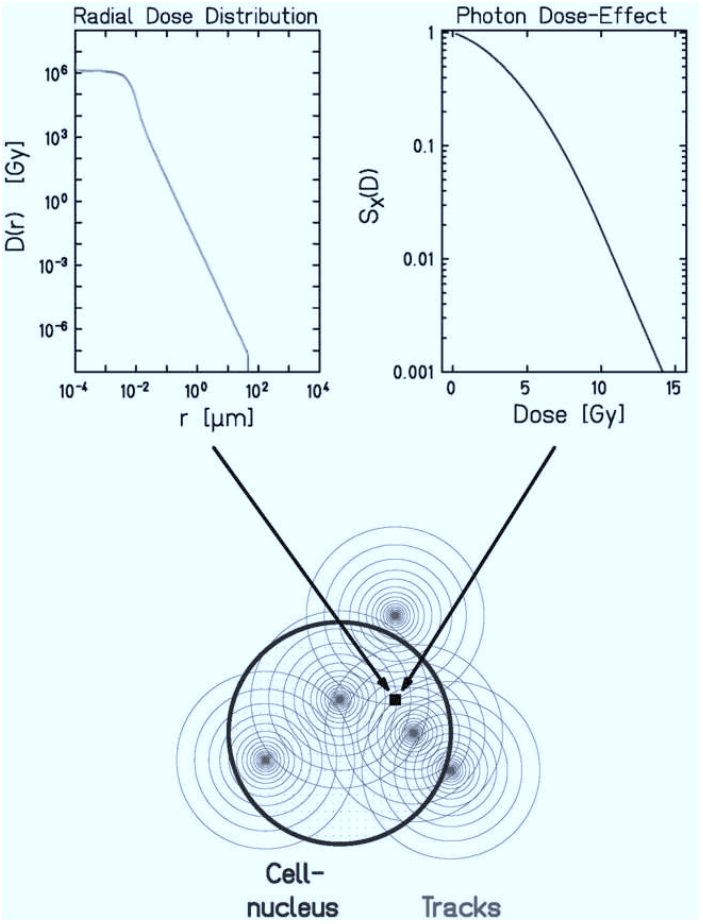

Figure 1. A sketch of the LEM and its three constituents, the radial dose distribution, the photon dose response curve and the cell nucleus as critical target.

we count SSB within a distance of 25 base pairs as an additional double strand break (DSB), we can define the damage enhancement factor η by

$$\eta = \frac{N(\mathrm{DSB}) + N(\mathrm{SSB} + \mathrm{SSB} = \mathrm{DSB})}{N(\mathrm{DSB})}, \tag{6}$$

where $N(\mathrm{DSB})$ is the number of DSB(s) for a certain dose according to the DSB yield after x-irradiation and $N(\mathrm{SSB} + \mathrm{SSB} = \mathrm{DSB})$ represents the additional damage due to SSB clustering. Therefore, we may write the survival curve in the following form:

$$S(D) = \begin{cases} \mathrm{e}^{-\alpha D - \beta D^2}, & D \leqslant D_\mathrm{t}, \\ S_t\, \mathrm{e}^{-s[\eta(D)D - D_\mathrm{t}]}, & D > D_\mathrm{t}, \end{cases} \tag{7}$$

where α, β denote the linear-quadratic components, $s = \alpha + 2\beta D_\mathrm{t}$ is the slope of the exponential tail for doses above D_t and S_t is the survival at the threshold dose D_t.

3. Radial dose distribution

The radial dose distribution around ion tracks plays a crucial role for the biological response, since it determines the initial distribution of lesions within the cell nucleus. All following

chemical and biological processes are based on the spatial pattern of ionization events induced by primary processes of the ions as well as secondary processes of ejected electrons. Hence, also the variety of the biological response for the same biological system can be attributed to the different ionization densities invoked by ions at different energies. In the following, we denote the primary energy distribution generated by the physical processes of target ionization and excitation on a timescale of 10^{-15} s with *initial dose distribution*. The subsequent chemical processes such as radical diffusion within the target medium are additionally taken into account for the calculation of the *actual dose distribution* or *track structure*.

3.1. Analytical descriptions of the initial dose distribution

The LEM requires an amorphous track structure description which can be either expressed by an analytical model or by the axial integration of the results of Monte Carlo simulations. In the first part, we summarize the analytical models under investigation. They are used in the different versions of the LEM [10, 21, 22] and in the MKM [23], where the track structure calculations are based on considerations by Kiefer and Chatterjee. All of them assume water as the relevant target and exploit the experimental results of gas chamber measurements that show a $1/r^2$-dependence of the initial dose distribution, if r describes the radial distance from the track centre. Although these experiments are not performed for liquid water or in tissue, one can well assume that this dependence also holds for the cell environment.

3.1.1. Constant track core radius. In the descriptions of the initial dose distribution used in the LEM, it is assumed that the track consists of an inner part with a constant initial dose attached to an outer part following a $1/r^2$-dependence. It can be expressed by

$$D(r) = \begin{cases} \lambda \,\mathrm{LET}/r_{\min}^2, & r < r_{\min}, \\ \lambda \,\mathrm{LET}/r^2, & r_{\min} \leqslant r \leqslant r_{\max}, \\ 0, & r > r_{\max}, \end{cases} \tag{8}$$

where LET denotes the linear energy transfer, λ is the normalization constant to assure that the radial integral reproduces the LET for a medium with density ρ:

$$\lambda = \frac{1}{\pi\rho\,[1 + 2\ln(r_{\max}/r_{\min})]}.$$

The maximum radius $r_{\max}$ is determined by those δ-electrons with the highest energy. It was found by Kiefer [24] that $r_{\max}$ only depends on the energy E (in MeV u^{-1}) and can be parameterized by

$$r_{\max} = \gamma\, E^{\delta}; \quad \gamma = 0.062\,, \quad \delta = 1.7, \quad r_{\max}\,\text{in}\,\mu\text{m},\ E\,\text{in MeV u}^{-1}$$

if the particle energy is above 1 MeV u^{-1}. The minimum or core radius $r_{\min}$ is different for the two different versions of the LEM, namely $r_{\min} = 0.3$ nm for the recent cluster version and $r_{\min} = 10$ nm for the original model. The latter uses the large radius to implicitly account for radical diffusion, whereas the novel version considers diffusion explicitly (see section 3.3).

3.1.2. Energy-dependent track core radius. In the previous subsection, we have assumed an energy-independent core radius. However, by applying Bohr's principle of adiabatic invariance to determine the core radius, we find that it depends on energy. Intuitively, we can understand that in the following way: for an energy transfer during ion–electron interaction, the ion transit time must be smaller than the reaction time of the target electron which is inversely proportional to the transferred energy. Hence, at a fixed target position, a fast ion implicates a short transit time and consequently a high possible energy transfer. As a result, the maximum distance below which the energy transfer is sufficient to ionize or excite a molecule increases for faster particles. Mozumder determined this maximum interaction range in condensed media between the ion and the target electrons by equating the outward flow of energy according to Fermi's theory to the neglected part of the stopping power arising from Bohr's principle of adiabatic invariance [25]. This derivation gives the following simple parameterization for the velocity dependent radius $r_{\min}$ of the inner part of the track:

$$r_{\min}(\beta_{\text{ion}}) = \beta_{\text{ion}} \cdot r_{\text{c}} \tag{9}$$

with $\beta_{\text{ion}} = v/c$, where v is the velocity of the particle, c is the speed of light and $r_{\text{c}} = 1.074\, c/(n\omega_0)$ describes the largest extension of the inner part of the track in the relativistic limit of $v = c$ with n being the refractive index of the medium and ω_0 the angular frequency associated with the ionization energy. For the case of liquid water, one can use $n = 1.33$ and $\omega_0 = 17\,\text{eV}\,\hbar^{-1}$ and find $r_{\text{c}} = 9.3\,\text{nm}$. Chatterjee *et al* [26] derived the maximum core radius in a similar way and found $r_{\text{c}} = 11.6\,\text{nm}$. We use this value throughout the paper for a better comparison with the Kiefer–Chatterjee (KC) model described in the next subsection.

In a recent approach of LEM, we analysed the carbon ion experiments of the radiation tolerance of the rat spinal cord, which is a well-accepted model system for normal tissue complications, with the assumptions of an energy-dependent track radius according to equation (9). Performing a χ^2-fit to the experimental data, we find that $r_{\text{c}} = 40\,\text{nm}$ gives the best agreement. Therefore, we also analyse the initial dose distribution using this phenomenologically derived maximum radius of the track core [22].

3.1.3. Kiefer–Chatterjee parameterization. The KC model combines the considerations for the maximum radius by Kiefer as already used in sections 3.1.1 and 3.1.2 with the Chatterjee approach for the minimum radius [26] as stated in equation (9). This description is used in a recent approach of the MKM [23]. The constant core dose D_{c} and the penumbra dose D_{p} as a function of track radius, r (μm), are given as follows:

$$D_{\text{p}}(r) = 1.25 \times 10^{-4} \left(\frac{z^*}{\beta_{\text{ion}}}\right)^2 r^{-2} \equiv K_{\text{p}} r^{-2} \quad [\text{Gy}], \tag{10}$$

$$D_{\text{c}} = \frac{1}{\pi\, r_{\min}^2} \left(\frac{\text{LET}}{\rho} - 2\pi\, K_{\text{p}} \ln\left(\frac{r_{\max}}{r_{\min}}\right)\right) \quad [\text{Gy}], \tag{11}$$

z^* is the effective charge given by the Barkas expression. The dose dependence in the penumbra expressed by equation (10) is determined by the classical collision dynamics. The constant core dose in equation (11) is normalized such that the radial integral of equations (10) and (11) yields the linear energy transfer. The core radius required to determine $r_{\min}$ was chosen to be $r_{\text{c}} = 11.6\,\text{nm}$.

3.1.4. Monte Carlo calculations of the initial dose distribution. In this section, we describe our second method under investigation, namely Monte Carlo simulations of the emission and transport of secondary electrons liberated during the transfer of a charged particle. The procedure is only briefly summarized here, for more details we refer to [12].

The mean free path between two primary interactions of heavy ions with the target material is determined from the total cross section of this process. The angular dependence of the emitted electrons is sampled according to the double differential cross section derived by the binary encounter approximation (BEA), and the energy dependence is taken according to Rudd's parameterization [27]. Subsequently, the track of each δ-electron is followed individually taking into account the three basic mechanism elastic scattering, ionization and excitation until the residual electron energy falls below 10 eV. In order to determine the absorbed dose the energy dissipated by the electrons is summed up along the ion's direction and divided by the volume under consideration. Additionally, we need to consider the dose deposited due to primary ionizations of the target in the track centre. Typically, about 30% of the total dose is dissipated due to primary ionization and excitation events in the track centre along the beam axis. Here, we assume that the ion's path follows a straight line and scattering during the stopping process is negligible. Moreover, we position the primary interaction events right on the ion trajectory at $r = 0$, thus neglecting the effects discussed in the previous section. For comparison with experimental data (see section 3.2), we follow the same procedure as in the experiments, where usually ionization events are measured and multiplied by the W value for the average energy transferred per ionization event.

3.1.5. Comparison of initial dose distributions. For the analysis, we compare the initial dose distributions based on equation (8) with a constant core radius of 0.3 nm (CR03), an energy-dependent core radius with $r_c = 11.6$ nm (EDR11) and 40 nm (EDR40), respectively, as well as the distributions for the KC model and the Monte Carlo simulations. The model CR03 is used in the cluster version of the LEM (LEM II) [21], the latest implementation of the LEM (LEM III) [22] uses EDR40, and EDR11 is taken for comparison with the KC approach, since both approaches rely on the same energy-dependent core radius. In figure 2, we show calculations for 300 and 11 MeV u^{-1} carbon ions in water (LET = 12.5 and 150 keV μm^{-1}), since these energies correspond to the typical energy in the entrance channel (normal tissue) and at the distal part of the spread-out Bragg peak (tumour volume), respectively. We can easily distinguish between the distributions of the different ion energies due to the larger central dose and the smaller radial extension of the slower ion. The maximum radius derived from MC calculations agrees quite well with the simple parametric energy scaling applied in the analytical models. Also the $1/r^2$-dependence for larger track radii holds for all representations. For the three models based on CR03, EDR11 and EDR40, we find similar absolute values for the penumbra region. For that part, the initial dose based on the KC representation shows the lowest dose. In general, the MC simulations yield doses between those based on equation (8) and the MC model.

Large differences are observed for the inner part of the ion track. Naturally, the dose for the simple analytical description (CR03, EDR11 and ER40) scales inversely to the core radius r_{min} spanning a dose range of three to four orders of magnitude. The larger central dose for CR03 compared to EDR40 is compensated for by the slightly smaller penumbra dose resulting in the same integral dose. The core dose derived from the KC description is more than one order of magnitude larger than the EDR11 with the same core radius. Finally, the highest local dose is observed by the MC simulations, where the energy due to primary events is assumed to be

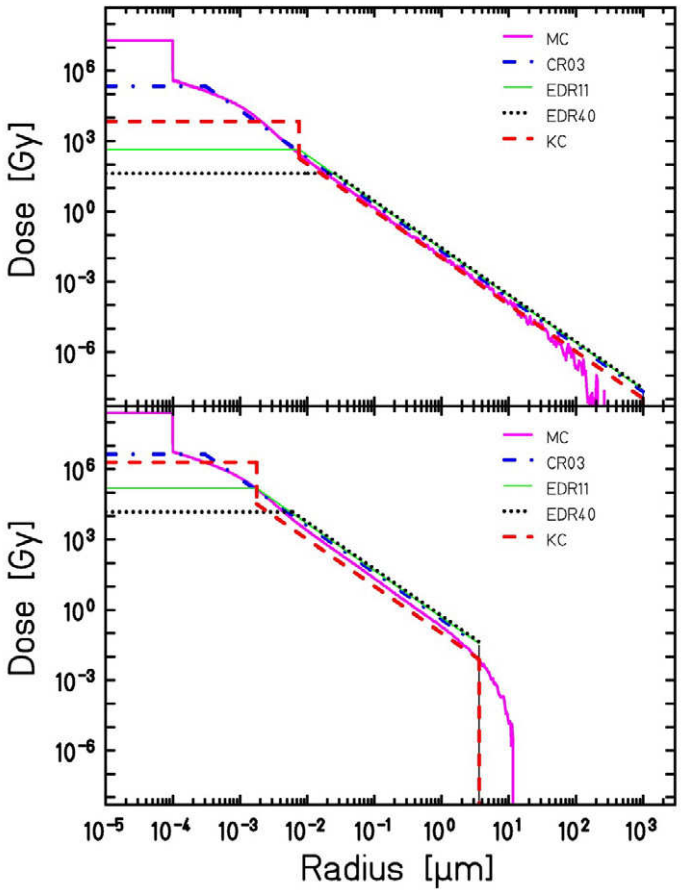

Figure 2. Initial dose distribution with a constant core radius (CR03, dashed-dotted line), with an energy dependent r_c of 11.6 nm (EDR11, thin solid line), and 40 nm (EDR40, dotted), and parameterized according to Kiefer and Chatterjee (KC, dashed line) compared to results obtained with Monte Carlo simulations (MC, thick solid line) for 300 MeV u^{-1} (upper panel) and 11 MeV u^{-1} (lower panel) carbon ions, respectively.

deposited on the ion track at $r < 10^{-4}$ μm. At most other radial distances the MC calculations agree with the simple analytical models except for the KC representation for 11 MeV u^{-1} carbon ions.

3.2. Comparison to experimental data

For modelling the biological response in ion therapy it is generally assumed that the irradiated medium is liquid water. However, the experimental determination of initial dose distributions in the liquid phase is extremely difficult and has not been performed yet. Therefore we need to use experimental data measured in the gas phase rescaled to match the density of liquid water. Varma *et al* [28, 29] carried out several such experiments. For the comparison depicted in figure 3, we chose two different data sets with low and high energy of oxygen and neon ions, respectively. This ion-energy combination closely relates to the typical clinical beams investigated in the previous subsection.

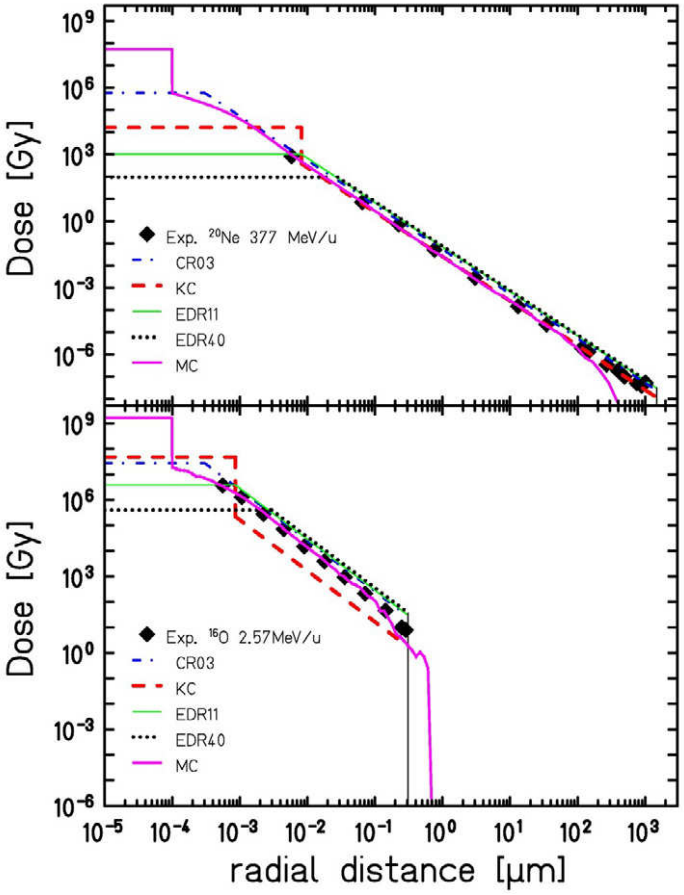

Figure 3. Upper panel: initial dose distribution of 377 MeV u^{-1} neon ions. Experimental data (diamonds) are taken from [29]. Theoretical curves are shown in the same representation as in figure 2. Lower panel: initial dose distribution of 2.57 MeV u^{-1} oxygen ions. Experimental data (diamonds) are taken from [28].

For 2.57 MeV u^{-1} oxygen ions, the initial dose distribution calculated by MC simulation agrees best with the experimental data. The distributions according to equation (8) are slightly too high in the penumbra region, whereas the dose description according to the KC representation falls almost one order of magnitude below the experimental results. In the track centre below 1 nm, only one data point is available, which shows that the KC model and the EDR40 representation deviate from the measurements.

For the high-energy Ne ions (377 MeV u^{-1}) all initial dose distributions agree rather well with the experimental data within the penumbra region. However, also here the theoretical values according to CR03, EDR11 and EDR40 slightly overestimate the local dose. For the core dose, we observe similar deviations as for the low-energy oxygen ions.

For the comparisons between experimental data and analytical models, we must bear in mind that the measurements only consider energy deposition due to ionization whereas excitation is neglected. Since about 10–15% of the absorbed energy is transferred to excitation, the local dose calculated by the analytical models must be considered too large relative to the

experimental data. Therefore, the deviations found in figure 3 are not surprising. For the Monte Carlo simulations, the ionization events can be explicitly modelled and multiplied by a constant W value representing the mean ionization energy in order to determine the corresponding dose deposition, thus the better agreement as observed in figure 3 could be expected.

3.3. Radical diffusion

Following the short physical stage ($<10^{-15}$ s), chemical processes start, where radicals that were created by interaction with primary ions or secondary electrons diffuse through the medium. They finally react with each other or with molecules in the irradiated medium such as sensitive sites of the DNA molecule. The radical diffusion length depends on the scavenging capacity and was determined to be $\sigma \approx 4$ nm for mammalian cells [30, 31].

In our calculations, the effect of radical diffusion is taken into account by convoluting the initial dose distribution $D(r)$ of equations (8), (10) and (11) and the discrete dose values of the Monte Carlo simulations, respectively, with a 2D Gaussian with the width of $\sigma = 4$ nm representing the radical diffusion:

$$f(r, r', \phi') = \frac{1}{2\pi\sigma^2} \mathrm{e}^{-(r^2 - 2rr'\cos\phi' + r'^2)/2\sigma^2} \tag{12}$$

where ϕ' denotes the angular coordinate.

Hence, the broadened actual dose distribution $\tilde{D}(r)$ can be calculated in the following way [32]:

$$\tilde{D}(r) = \int_0^\infty \mathrm{d}r' r' \int_0^{2\pi} \mathrm{d}\phi' D(r') f(r, r', \phi') = \frac{\mathrm{e}^{-r^2/2\sigma^2}}{\sigma^2} \int_0^\infty \mathrm{d}r' r' \mathrm{e}^{-r'^2/2\sigma^2} I_0\left(\frac{rr'}{\sigma^2}\right) D(r'), \tag{13}$$

where I_0 denotes the modified Bessel function of order zero.

In figure 4, we compare the actual dose distributions $\tilde{D}$ for all models considered in the previous subsections and find that the large dose differences in the track centre of five orders of magnitude as depicted in figure 2 are largely diminished to within two orders of magnitude. The highest local dose in the track core is provided by the Monte Carlo code and the KC dose representation followed by the four different representations of the analytical model according to equation (8). Notably, the actual dose distribution CR03, which shows the second-largest local doses in figure 2, gives lower values when considering radical diffusion relative to the MC simulations and the KC model. The reason is that the large doses of CR03 occur only in a very small region around the track centre, whereas in the KC model the lower maximum dose is spread over a much larger area. In general, the broadening of the radial dose only affects the inner part of the ion track with $r < 20$ nm, the largest part of the penumbra remains the same as in figure 2. Additionally, we included the track structure model of the original version (LEM I) of the LEM (CR10) into figure 4, where the radical diffusion was integrated into the 'initial' dose distribution. For this representation, we find the lowest core dose of all models for the low-energy beam and also relatively low core doses for the high-energy ions.

4. Application of the LEM

The assessment of the different actual dose distributions in terms of biological effects requires the integration into the LEM. The calculation of cell inactivation probabilities expressed by the

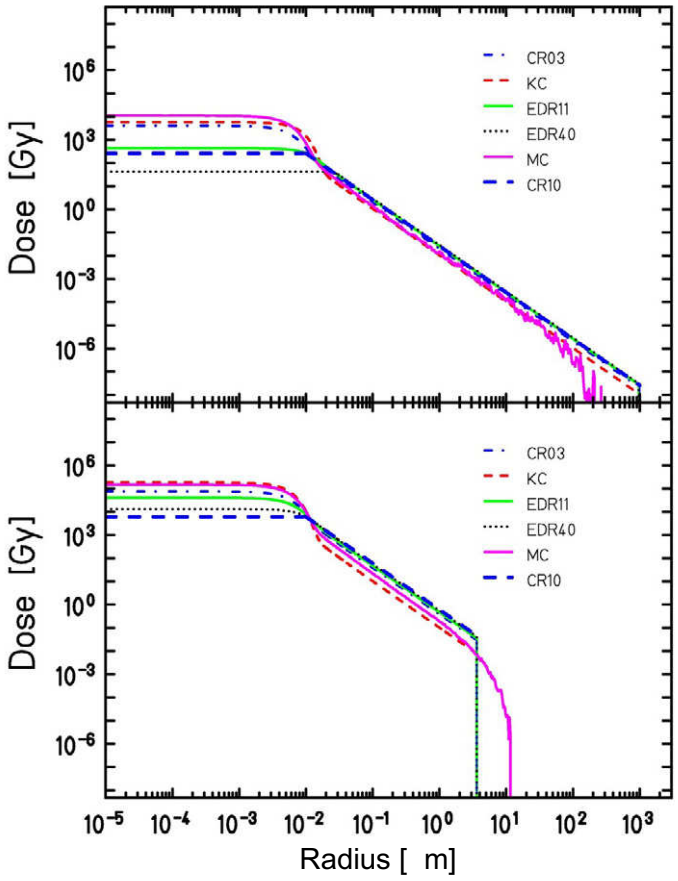

Figure 4. Actual dose distribution $\tilde{D}$. The curves of figure 2 are convoluted with a 2D Gaussian distribution to account for radical diffusion. They are shown for the same energies (upper panel 300 MeV u^{-1}, lower panel 11 MeV u^{-1} carbon ions, respectively) and in the same presentation as in figure 2. The original dose distribution used in the LEM (CR10) is depicted as dark dashed line.

initial slope α_I of the ion dose response curve is required in treatment planning systems for ion therapy and therefore it is of utmost importance. In the following, we apply the approximation described in [10] for a rapid calculation of cell inactivation. The results for RBE calculations of the initial slope of the survival curve for the standard HSG cell line following carbon irradiation are depicted in figure 5. We use the parameters of [21] for the cluster version of the LEM ($\alpha = 0.313\,\mathrm{Gy}^{-1}$, $\beta = 0.0615\,\mathrm{Gy}^{-2}$, $r_n = 5\,\mu$m and $D_t = 6\,$Gy), which were shown to give the best fit (based on χ^2-analysis) to the experimental data. The cluster version uses the CR03 model. The implementations EDR11 and EDR40 give much smaller data for the initial RBE, whereas the application of the actual dose distribution based on the Monte Carlo code and on the Kiefer and Chatterjee representation, respectively, yields very high initial slopes. If we compare these results with the findings of figure 4, we can conclude that the inner part of the ion tracks is decisive for the slope of the survival curve and hence for cell inactivation. Although the larger energy deposition in the track centre for the KC and MC models is compensated for

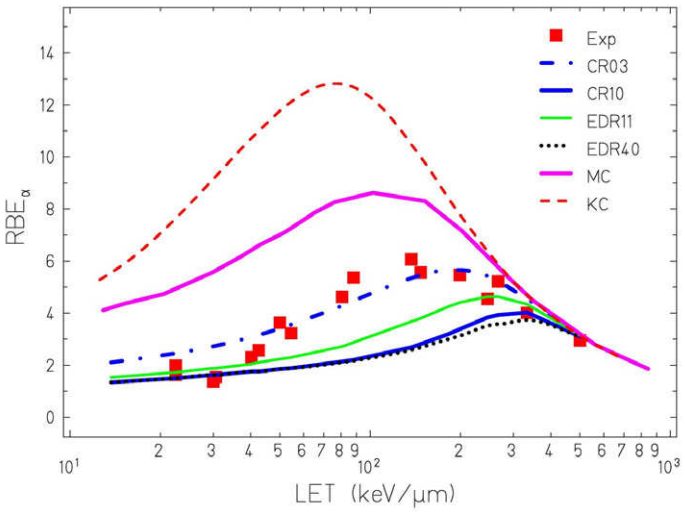

Figure 5. Initial slope α as predicted by the LEM for the different actual dose distributions of figure 4 applied to the experimental data by Furusawa *et al* for HSG cells. Model parameters: $\alpha = 0.313\,\mathrm{Gy}^{-1}$, $\beta = 0.0615\,\mathrm{Gy}^{-2}$, $r_\mathrm{n} = 5\,\mu\mathrm{m}$ and $D_\mathrm{t} = 6\,\mathrm{Gy}$.

by lower doses in the penumbra, the pronounced nonlinear behaviour of the underlying photon survival curve according to equation (7) for large local doses results in these high values for the RBE. The curve for the original version of the LEM underestimates the experimental data only because in that model version cluster effects, represented by the factor η in equation (7), were not taken into account.

The impact of local doses in the core is strongly related to the high dose part of the photon dose response curve used to translate the effects of ions to those of photons. In the LEM approach, it is mainly determined by the value of the threshold dose D_t. In figure 6, we show the results of the different track structure models using an optimal parameter D_t. All radial distributions can be used to reasonably fit the experimental data. However, the threshold parameters determined for the KC ($D_\mathrm{t} = 0.01\,\mathrm{Gy}$) and MC ($D_\mathrm{t} = 1.6\,\mathrm{Gy}$) models are not realistic, since the experimental data of the x-ray measurements unambiguously show that the survival curve does not turn to a purely exponential function at such low doses.

From the experimental data depicted in figure 6 we can determine that the ratio of α_I for high-LET particles relative to low-LET radiation is about 4. All model predictions result in a slightly smaller ratio, where the original LEM (CR10) exhibits the smallest and the EDR40 the largest values, respectively. In general, the agreement for high-LET particles representative for the radiation quality in the extended Bragg peak covering the tumour volume is well reproduced. However, all track structure versions applied in this paper yield too steep initial slopes for low-LET particles. We also calculated the uncertainties of the initial RBE with respect to the most critical parameter D_t for energies (or LET values) representing the two most interesting cases for treatment planning, namely the entrance channel ($13\,\mathrm{keV}\,\mu\mathrm{m}^{-1}$) and a typical position at the distal part of the spread-out Bragg peak ($77\,\mathrm{keV}\,\mu\mathrm{m}^{-1}$). The RBE values for the cases depicted in figure 6 are summarized in table 1. The uncertainties are determined by a variation of D_t by $\pm 10\%$ as in the discussion presented in a previous paper [22]. In general, the change of the threshold parameter by 10% introduces a deviation of the RBE by about 5%. Only for the KC

Table 1. RBE values and uncertainties for the cases considered in figure 6 for 13 keV μm^{-1} (entrance channel) and 77 keV μm^{-1} (spread-out Bragg peak) particles. The uncertainties were determined by varying D_t by $\pm 10\%$.

Dose distribution	CR03	CR10	EDR40	MC	KC
13 keV μm^{-1}	2.12 ± 0.1	2.6 ± 0.11	1.72 ± 0.03	2.18 ± 0.08	1.68 ± 0.01
77 keV μm^{-1}	4.22 ± 0.23	4.5 ± 0.25	4.35 ± 0.25	4.64 ± 0.15	5.24 ± 0.01

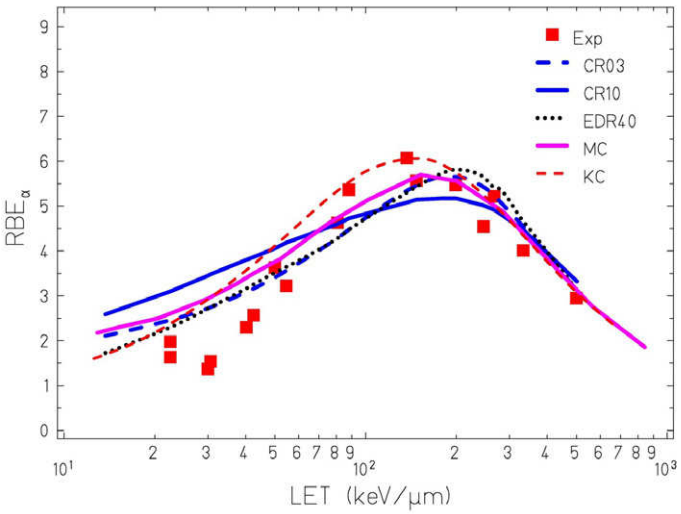

Figure 6. Initial slope α as predicted by the LEM for the different actual dose distributions of figure 4 applied to the experimental data by Furusawa *et al* for HSG cells. Model parameters: $\alpha = 0.313\,\text{Gy}^{-1}$, $\beta = 0.0615\,\text{Gy}^{-2}$ and $r_n = 5\,\mu$m. The threshold parameter D_t was varied in order to fit the experimental data. $D_t = 6\,$Gy(CR03), $D_t = 23\,$Gy(EDR40), $D_t = 1.6\,$Gy(MC), $D_t = 30\,$Gy(CR10) and $D_t = 0.01\,$Gy(KC).

track structure, no influence of D_t is found. This fact is not surprising since the unrealistic value of 0.01 Gy is so low that basically a linear shape of the photon response curve is assumed.

5. Discussion

The results of the previous sections clearly demonstrate the significance of the inner part of the ion track. Although the agreement with experimental data is reasonable for all different initial dose distributions (figure 3) at larger radii, the differences of the distributions in the track core yield large variations in the corresponding RBE calculations for cell inactivation (figure 5). The integration of radical diffusion into the model calculations diminishes the differences, but also in this case the core dose spreads over more than two orders of magnitude for particles with the same energy (figure 4). Considering the results of figure 6, we find that the LEM gives good results for all track structure models by choosing the threshold parameter D_t appropriately.

Therefore, the local damage expressed by the integrand of equation (5) is the crucial quantity. It includes both the actual dose distribution and the photon response curve. However, the threshold parameter and the local dose in the track core need to be consistent with experimental data. In this work, we have shown that the existing track structure models agree with these data, but the assumptions about D_t are not in line with the measurements for all models, since the MC and KC representations require threshold parameters that are too low in comparison with the experimental data of the photon survival curve. Due to the otherwise general good agreement of the LEM with experimental data, we can conclude that the extremely large local doses (despite broadening by diffusion) are incompatible with the biological experimental data. They originate from the initial assumptions made in these approaches. For example, for the MC model discussed here, it is assumed that the primary ionizations occur at the track centre ($r = 0$). For the KC approach, the chosen partition of dose between the core and penumbra might result in doses that are too high in the core.

The strong dependence of the RBE values on the track core is a specific feature of the LEM, since it assumes that the biological response is determined by the damage in very small regions of the order of nanometres. This is in accordance with experiments with ultrasoft x-rays, where the relevant scale was found to be on the nanometre scale [33]. The clustering of damage on the scale of a few tens of base pairs seems to be at least as important as interactions at larger distances [34]. However, models also exist that are based on the latter assumptions. Especially, the recent MKM shows promising results in terms of accuracy and diversity possibly applicable for heavy ion treatment planning. Our analysis shows that the core dose of the KC model used in the MKM might be overestimated. However, in the MKM, the biological damage (average number of lethal events) is determined by the dose mean specific energy in small domains with a radius of about 0.3–0.5 μm yielding a dose-weighted mean of the deposited energy. This procedure largely flattens the actual dose in the target, which is used to derive the biological effect from the photon reference curve. For the same reason, the radical diffusion is of little importance, since diffusion over nanometre distances is negligible compared to the averaging over micrometre distances. A different approach that uses an amorphous track structure was proposed by Katz [18]. In that model, two different inactivation modes, namely ion-kill and gamma-kill, are distinguished. Similar to the MKM model, for the ion-kill mode the dose is averaged over domains with an extension on the order of micrometres, neglecting the dose variations on the nanometre scale.

Surprisingly, all three models are able to represent experimental inactivation data with reasonable agreement, and it is thus instructive to elaborate on the different generation of the biological response based on the specific model assumptions. The lower averaged target dose in the MKM and Katz model in comparison to the high local dose in the LEM must be compensated by a different assumption about the effectiveness of the large ionization density. In the MKM, the photon dose response curve is assumed to be represented by the linear-quadratic model without transition to an exponential shape at high doses. Consequently, the lower target dose in the MKM is compensated by a higher effectiveness of the photon reference curve, finally leading to similar predictions for the effectiveness of particle radiation as compared to the LEM. The Katz model uses a different way to treat the high damage invoked by the high-energy deposition in the track as expressed in the contribution of the ion-kill mode. This ion-kill mode is represented by an exponential dose response that can be related to the multi-target single-hit formalism in terms of the model parameter κ [35]. The introduction of the

parameter κ corresponds to an increased final slope of the photon dose response curve with a higher effectiveness as compared to the experimental data.

6. Conclusion

We compared different amorphous track structure representations and showed that they nearly coincide at large distances from the trajectory, whereas they significantly differ at small radii in the track centre. We further investigated the significance of the local dose in the inner part of ion tracks for the calculation of RBE values for cell inactivation. Therefore, we applied the LEM using several amorphous track structure models. Despite the large differences in the core region, the resulting RBE values agree surprisingly well, if the threshold parameter D_t is varied to allow for a good representation of the experimental data. However, the range of reasonable D_t values is limited and does not cover values necessary to generate reasonable results for some models. Moreover, the ratio of the RBE values for high versus low LET particles also depends on the track structure. This relation is directly linked to the therapeutic ratio of the biologically effective dose in the tumour region relative to the biologically effective dose in normal tissues. Although the LEM predicts the cell inactivation for particles with an LET above 50 keV μm^{-1} with an excellent accuracy, the predicted values for low-LET particles are significantly overestimated. Earlier comparisons for lighter particles showed the same trend of deviation between model calculations and experimental data [21]. As a consequence thereof, the real therapeutic ratio is expected to be higher than calculated with the LEM. Therefore, it is of utmost interest to further study ion–matter interaction in liquid water over the entire range of therapy-relevant specific energies between 1 and 400 MeV u^{-1}. Simultaneous theoretical and experimental studies are required to further investigate in particular the local dose at very small distances from the track centre, which is expected to dominate the biological effectiveness of charged particles.

References

[1] Kraft G 2000 *Nucl. Instrum. Methods Phys. Res.* A **454** 1–10
[2] Schulz-Ertner D, Karger C P, Feuerhake A, Nikoghosyan A, Combs S E, Jakel O, Edler L, Scholz M and Debus J 2007 *Int. J. Radiat. Oncol. Biol. Phys.* **68** 449–57
[3] Schulz-Ertner D, Nikoghosyan A, Hof H, Didinger B, Combs S E, Jakel O, Karger C P, Edler L and Debus J 2007 *Int. J. Radiat. Oncol. Biol. Phys.* **67** 171–7
[4] Amaldi U and Kraft G 2007 *J. Radiat. Res. (Tokyo)* **48** (Suppl A) A27–41
[5] Weyrather W K, Ritter S, Scholz M and Kraft G 1999 *Int. J. Radiat. Biol.* **75** 1357–64
[6] Karger C P, Peschke P, Sanchez-Brandelik R, Scholz M and Debus J 2006 *Int. J. Radiat. Oncol. Biol. Phys.* **66** 1488–97
[7] Lyman J T, Howard J, Kanstein L and Alonso J R 1980 *Biological and Medical Research with Accelerated Heavy Ions at the Bevalac, 1977–1980* ed M C Pirucelli and C A Tobias (Berkeley, CA: University of California) LBL 11220, UC-48, pp 319–24
[8] Kanai T *et al* 1999 *Int. J. Radiat. Oncol. Biol. Phys.* **44** 201–10
[9] Scholz M and Kraft G 1994 *Radiat. Prot. Dosim.* **52** 29–33
[10] Scholz M, Kellerer A M, Kraft-Weyrather W and Kraft G 1997 *Radiat. Environ. Biophys.* **36** 59–66
[11] Nikjoo H, O'Neill P, Terrissol M and Goodhead D T 1994 *Int. J. Radiat. Biol.* **66** 453–7
[12] Krämer M and Kraft G 1994 *Radiat. Environ. Biophys.* **33** 91–109
[13] Paretzke H G, Turner J E, Hamm R N, Ritchie R H and Wright H A 1991 *Radiat. Res.* **127** 121–9
[14] Cucinotta F A, Nikjoo H and Goodhead D T 1999 *Radiat. Environ. Biophys.* **38** 81–92

[15] Furusawa Y, Fukutsu K, Aoki M, Itsukaichi H, Eguchi-Kasai K, Ohara H, Yatagai F, Kanai T and Ando K 2000 *Radiat. Res.* **154** 485–96
[16] Hawkins R B 2003 *Radiat. Res.* **160** 61–9
[17] Kase Y, Kanai T, Matsumoto Y, Furusawa Y, Okamoto H, Asaba T, Sakama M and Shinoda H 2006 *Radiat. Res.* **166** 629–38
[18] Katz R, Ackerson B, Homayoonfar M and Sharma S C 1971 *Radiat. Res.* **47** 402–25
[19] Scholz M and Kraft G 1996 *Adv. Space Res.* **18** 5–14
[20] Fertil B, Reydellet I and Deschavanne P J 1994 *Radiat. Res.* **138** 61–9
[21] Elsässer Th and Scholz M 2007 *Radiat. Res.* **167** 319–29
[22] Elsässer T, Krämer M and Scholz M 2008 *Int. J. Radiat. Oncol. Biol. Phys.* **71** 866–72
[23] Kase Y, Kanai T, Matsufuji N, Furusawa Y, Elsässer T and Scholz M 2008 *Phys. Med. Biol.* **53** 37–59
[24] Kiefer J and Straaten H 1986 *Phys. Med. Biol.* **31** 1201–9
[25] Mozumder A and Magee J L 1974 *J. Chem. Phys.* **60** 1145–8
[26] Chatterjee A and Schaefer H J 1976 *Radiat. Environ. Biophys.* **13** 215–27
[27] Rudd M E 1988 *Phys. Rev.* A **38** 6129–37
[28] Varma M N, Baum J W and Kuehner A V 1977 *Radiat. Res.* **70** 511–8
[29] Varma M N and Baum J W 1980 *Radiat. Res.* **81** 355–63
[30] Nikjoo H, O'Neill P, Goodhead D T and Terrissol M 1997 *Int. J. Radiat. Biol.* **71** 467–83
[31] Moiseenko V V, Hamm R N, Waker A J and Prestwich W V 2001 *Radiat. Environ. Biophys.* **40** 23–31
[32] Brons S, Taucher-Scholz G, Scholz M and Kraft G 2003 *Radiat. Environ. Biophys.* **42** 63–72
[33] Goodhead D T, Thacker J and Cox R 1979 *Int. J. Radiat. Biol. Relat Stud. Phys. Chem. Med.* **36** 101–14
[34] Rossi H H and Zaider M 1991 *Med. Phys.* **18** 1085–92
[35] Katz R and Sharma S C 1973 *Nucl. Instrum. Methods* **111** 93–116